

The Cosmic-Ray Dominated Region of Protoplanetary Disks

G. Chaparro Molano and I. Kamp

Abstract We investigate the chemical evolution in the midplane of protoplanetary disks in the region $1 \text{ AU} \leq r \leq 10 \text{ AU}$, focusing on cosmic ray induced processes. These processes drive the chemical pathways of formation of gas phase molecules which later can be adsorbed onto the surface of grains. We improve on previously existing chemical models by treating the interaction of cosmic rays with the gas/grain environment in a way that is consistent with the local conditions. This means including the effects of dust aggregation in the disk and the extinction of cosmic ray induced UV photons by the gas. We conclude that the effects of cosmic ray UV flux enhancement brought about by grain growth are as relevant as their extinction by gas species. Thus we identify CO, CO₂, SiO, S and O₂ as the main species that contribute to the gas extinction in these regions. The implementation of this method seeks to complete other models that use steady state estimations of the chemical composition of the disk.

1 Introduction

Cosmic rays play a role in ionizing the material and driving the chemistry in protoplanetary disks, which has been largely underestimated. This is specially true in the region where they can be most relevant: the cold environment of the midplane of protoplanetary disks. This region is known to be opaque to stellar UV and X ray photons [27] and for this reason it has the reputation of being a dead zone. However, the region of the midplane located at $z/r < 0.05$ and $1 < r < 10 \text{ AU}$ can in fact be dominated by cosmic ray processing, as they penetrate above column densities of $\Sigma \sim 150 \text{ g cm}^{-2}$ [19, 23]. Steady state chemical models applied to

G.C. Molano (✉) · I. Kamp
Kapteyn Astronomical Institute, Postbus 800, 9747 AV Groningen, The Netherlands
e-mail: chaparro@astro.rug.nl

these regions cannot fully describe the chemical evolution of the midplane, as the chemical relaxation timescale can be up to 10^8 years [27], which is longer than the lifetime of the disk [9].

Current chemical models of protoplanetary disks do include to a large extent the effects of cosmic rays [18, 22, 24–27]. However, the effects of the local gas opacity and grain growth are for the most part overlooked, as the parameters for estimating cosmic ray photoionization/dissociation rates are usually taken from molecular cloud literature [10, 28].

Our goal is to identify the main contributors to the extinction of cosmic ray induced UV (CRUV) photons in different regions of the midplane ($r = 1\text{--}10$ AU) of a disk of a T Tauri star. We implement a time dependent calculation of the CRUV photo rates that includes the extinction provided by the dust and also by gas species, which depend on their relative abundances. We implement this method in our time dependent chemical rate equation solver `chem_compact`. This code is benchmarked against steady state chemical abundances from the PRODIMO solver [27] and against observed cometary ice abundances [4, 7].

2 Cosmic Ray Induced UV Photons

Besides direct ionization of gas phase species cosmic rays can ionize the medium by inducing a UV field that comes from secondary ionization of molecular hydrogen. The process, known as the Prasad Tarafdar mechanism [15], starts when an electron, with a typical energy of 30 eV, is released after the cosmic ray ionization of an H_2 molecule. This electron then hits another (neutral) H_2 molecule, which leaves it in an excited electronic state [16, 21]. The emission probability profile of CRUV is obtained from the transition probability of the first three excited electronic levels ($B^1\Sigma_u^+$ and $C^1\Sigma_u$). In the subsequent decay to excited vibrational states of the ground electronic level, Lyman and Werner photons are emitted in the 90–170 nm range.

Cosmic ray induced UV photons can be absorbed by the material in the local environment where they are generated. Both gas and dust can absorb these photons and become a source of local extinction, but this depends on the local density and temperature conditions. For instance, at 10 AU most of the material is frozen on the surface of dust grains and therefore the extinction of CRUV depends entirely on the local dust properties. Thus, in such gas poor environments the CRUV photoprocesses will not be affected by the composition of the gas and the chemistry can be described in a fairly straightforward way.

The rate of CRUV photoprocesses depends on the shape of the photon emission probability from every cosmic ray ionization of H_2 :

$$k_{\text{CU},i} = \zeta_{\text{H}_2} \frac{n_{\text{H}_2}}{n_{\langle\text{H}\rangle}} \gamma_i ; \quad \gamma_i = \int_{1.76\text{PHz}}^{3.28\text{PHz}} \frac{P(\nu)\sigma_i(\nu)}{\sigma_{\text{tot}}(\nu)} d\nu . \quad (1)$$

P is the emission probability profile of a CRUV photon, σ_i is the photoprocess cross section, and σ_{tot} is the total (gas+dust) cross section. This cross section includes the information of the relative gas abundances and cross sections of all other gas phase species. This expression implicitly includes a shielding effect, which can be important in regions where high density/temperature combinations create a gas rich environment. From Eq. (1) we can define the frequency averaged opacity as:

$$\langle \kappa_i \rangle = \frac{\int F(\nu) \kappa_i(\nu) d\nu}{\int F(\nu) d\nu}. \quad (2)$$

The shape of the radiation field that dissociates or ionizes a species $F(\nu)$ not only depends on the CRUV emission probability, but also on the CRUV extinction of all other species $\sigma_{\text{tot}}(\nu)$, which leads to the frequency dependent opacity $\kappa_i(\nu)$:

$$F(\nu) = \frac{P(\nu)}{\sigma_{\text{tot}}(\nu)}; \quad \kappa_i(\nu) = \xi_i \sigma_i(\nu) \frac{n_{\text{(H)}}}{\rho_{\text{gas}}}. \quad (3)$$

Here $\rho_{\text{gas}} = n_{\text{(H)}} \mu m_{\text{H}}$ (μ being the mean molecular weight). This formula for the opacity yields units of cm^2 per gram gas. Using Eq. (3) the expression for the opacity can be rewritten as:

$$\langle \kappa_i \rangle = \frac{\xi \gamma_i}{\gamma_0 \mu m_{\text{H}}}; \quad \gamma_0 = \int \frac{P(\nu)}{\sigma_{\text{tot}}(\nu)} d\nu. \quad (4)$$

The grain size distribution in a protoplanetary disk has larger grains in protoplanetary disks than in molecular clouds because of grain growth [8]. An increase in the average grain size will decrease the combined area per unit volume, which means that grains will become less efficient in absorbing incoming UV photons. From a typical protoplanetary disk dust size distribution $f(a) \sim a^{-p}$, where a is the dust radius ($0.1 \mu\text{m} \leq a \leq 10 \mu\text{m}$) we calculate the maximum CRUV photon flux in a gas poor region of a protoplanetary disk to be $N_{\text{CU}} \simeq 386,000 \text{ photons cm}^{-2}\text{s}^{-1}$. This value is 40 times larger than in molecular clouds, compared to previous estimates of $10^4 \text{ photons cm}^{-2}\text{s}^{-1}$ [20].

3 Chemical Model

The code `chem_compact` is our VODE based [5] gas/grain chemical rate equation solver. In it we include a reaction network based mostly on the UMIST06 database for astrochemistry [28] and including H_2 formation on grains [6] and ad/desorption reactions: Adsorption and thermal and stellar UV photodesorption from [2, 13, 14], cosmic ray direct and induced UV photo-desorption from [11, 17]. We consider 67 chemical species composed of 8 elements.

Table 1 Physical conditions in relevant gas rich-regions, from the PRODiMO simulation [27]

r (AU)	T (K)	$n_{\text{(H)}}$ (cm^{-3})
1	80	10^{14}
3–5	65	10^{12}
7–8	40	10^{11}

The initial conditions for our disk model were obtained by running our chemical evolution code under molecular cloud conditions ($T = 20$ K, $n_{\text{(H)}} = 10^6 \text{ cm}^{-3}$) from atomic, low metallicity abundances. The resulting abundances after 10^7 year were used as initial conditions. We use low metal initial abundances because Si, Fe, and Mg form dust grains before the formation of the disk.¹

In order to estimate the effects of gas opacity in the CRUV photoprocess rates and therefore in the chemical evolution, we replace the relevant rates from the UMIST [28] database with our own rates, Eq. (1). As these rates depend on ξ_i , we recalculate them at every timestep as the solver yields new values for the gas abundances.

3.1 Chemistry in Gas-Rich Regions

The gas-rich regions of the disk probed in our models are listed in Table 1. In the regions studied, the dominant species are CO (gas) and H₂O (ice) consistently, while O₂, O, SiO, CO₂, and CH₄ are the secondary carriers of carbon, silicon and oxygen. The opacity is mostly provided by O₂, SiO, CO₂, and S, where SiO and O₂ are the species that dominate the opacity. From Figs. 1 and 2 we can see that the evolution of SiO and O₂ correspond to changes in the opacity. For this reason, here we will showcase the interaction between those species. We can see that the correlation between the chemical evolution and the opacity is very complex, and the variations are not linear in nature. This shows that the chemical evolution obtained when considering the effects of gas opacity is not simply halfway between low and a high CRUV field conditions, but it has to be studied in a case by case basis.

In Fig. 2 we can see that at 1 AU after 10^4 year the gas opacities rise, while the dust opacity remains constant. The late O₂ enhancement seen in Fig. 1 implies that it is providing most of the CRUV gas extinction, and thus SiO absorbs less CRUV photons. Thus, as the opacity fraction provided by dust grains is reduced, O₂ self shields and it slows down atomic oxygen formation via photodissociation of SiO. This causes a rebound effect after 10^5 year, as O₂ needs a constant supply of atomic oxygen for its formation.

At 3–5 AU from the central star the temperature is lower than at 1 AU. Thus, SiO is now mostly in the ice phase, while retaining a small presence in the gas. It is kept at a stable but low level throughout the simulation. This implies that OH

¹This is what sightlines show where the absorption lines of these metals are measured from various clouds against a bright background star [12].

Fig. 1 Chemical abundance evolution

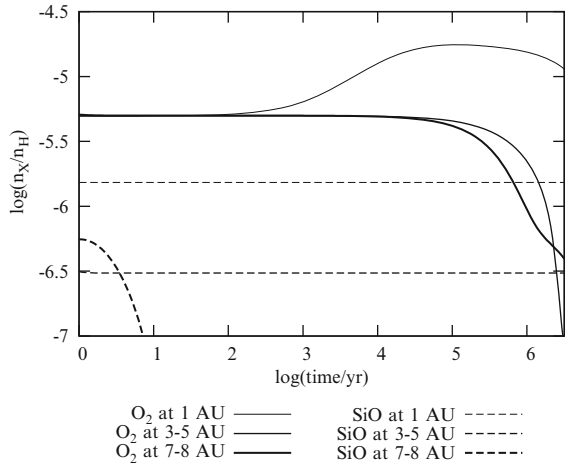
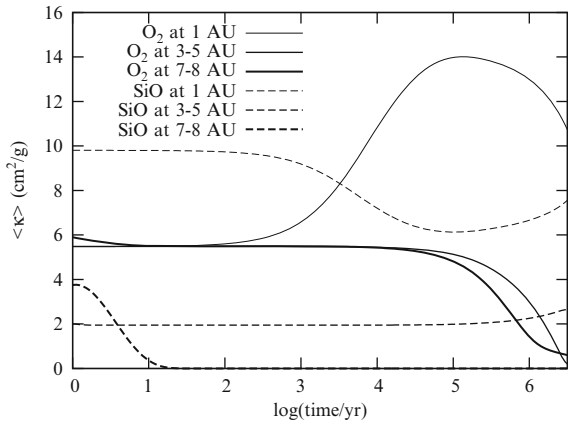


Fig. 2 CRUV gas opacity vs. time. For reference, the dust opacity is $68 \text{ cm}^2/\text{g}$ (gas)



formation from SiO is not as efficient as it was at 1 AU. The low OH formation rate cannot sustain the formation of O₂ because the oxygen in it is lost to H₂O. The consequent decrease in O₂ opacity causes the CRUV photorates to increase for other molecules, as it allows more CRUV photons to dissociate or ionize other species. This is evidenced in Fig. 2, as the SiO opacity increases as the O₂ opacity decreases. Now CH₄ CRUV photodissociation becomes very efficient at forming CH₂, which reacts with OH faster than any other OH reaction. This exacerbates the depletion of O₂, as seen at the end of the simulation in Fig. 1. The gas opacity in this region is about a third less than in the 1 AU region, which is caused by the lack of efficient O₂ formation and the freeze out of SiO.

As we can see from the chemical evolution plot in Fig. 1, at 7–8 AU SiO is completely frozen after only 1 year, with negligible gas phase abundances, even though the chemical evolution for the other significant species remains more or less the same. However, the lack of SiO in the gas phase impacts the late formation of

H₂O that appears at lower distances. Since O₂ is not consumed in the formation of water, its depletion is not as dramatic as in the 3–5 AU region. The gas opacity here is very similar to that observed at 3–5 AU (Fig. 2), except for the absence of SiO opacity due to freeze out, which enhances the CRUV rates for all other species, including CO.

The longevity granted to SiO in our efficient CRUV induced OH formation models in the disk midplane has repercussions beyond the midplane of the disk. Following [1], the vertical drift timescale τ_{vd} of a molecule that moves up to a distance $z = \lambda$ above the midplane can be estimated using the disk viscosity. A simple calculation for $\lambda = 0.1$ AU, corresponding to the $A_V = 1$ region (at $r = 1$ AU) of the disk yields that $\tau_{\text{vd}} \simeq 280$ year. An SiO molecule can survive for approximately 10^3 year (if $\chi = 1$) or 1 year (if $\chi = 10^3$) before being photodissociated by the stellar UV field at the $A_V = 1$ region. Therefore, in the optimistic (former) case it is possible for SiO to accumulate around $A_V = 1$ and to be detectable. However, since the region where SiO is being formed has a small radial extent ($r \leq 1 - 5$ AU), its detection could prove to be very difficult.

3.2 Chemistry at 10 AU

In this region the environment is cold enough (20 K, at a density of 10^{10} cm^{-3}) to allow us to study the chemical evolution without taking into account the gas opacity [7]. Under these conditions, the CRUV rate constant takes the familiar form:

$$k_{\text{CU},i} = \frac{\xi_{\text{H}_2}}{\sigma_{(\text{H})}^{\text{UV}}(1 - \omega)} \int_{1.76 \text{ PHz}}^{3.28 \text{ PHz}} P(\nu) \sigma_i(\nu) d\nu. \quad (5)$$

This is the expression that is frequently used in models that include CRUV photoprocesses [10, 21, 28], mostly because it is valid for ISM and molecular cloud conditions (low gas abundances). This formula is very convenient for computing the chemical rate equations, as everything in the rate constant can be calculated beforehand.

After 10^6 years the ice content resembles what is observed in cometary ices [3, 4], where H₂O ice is followed by CO and CO₂ ice and, to a lesser degree, CH₄ ice. In our model, CH₄ ice is formed only after water ice formation has become so efficient that it takes away most of the oxygen from CO and leaves the carbon free to form other molecules. This suggests that the CH₄ ice found in comets may have been formed at a late stage of the disk evolution.

We present a comparison between measured cometary ice abundances and our resulting ice abundances in Table 2. Our resulting ice ratios are very close to the cometary values when using a cometary carbon-to-oxygen ratio. This happens because a fraction of the total carbon may be stored in the core of dust grains in our model. These results fit the cometary $n_{\text{CO}\#}/n_{\text{H}_2\text{O}\#}$ and $n_{\text{CO}_2\#}/n_{\text{H}_2\text{O}\#}$ ratios closely, which means that the relative abundances of ice species can be predicted by our model.

Table 2 Ice ratios in comets compared to our results

Ratio	Cometary measurements ^a	c_{-c}^b : [C/O] = 0.16 10 ⁷ year
$n_{\text{CO}_2\#}/n_{\text{CO}\#}$	<0.6	0.43
$n_{\text{CO}\#}/n_{\text{H}_2\text{O}\#}$	<0.2	0.14
$n_{\text{CO}_2\#}/n_{\text{H}_2\text{O}\#}$	0.02–0.12	0.06
$n_{\text{CH}_4\#}/n_{\text{H}_2\text{O}\#}$	0.003–0.015	<0.001

^a Abundances compiled from cometary measurements in [3,4]

^b Ratios from our `chem_compact` model

4 Conclusions

We have included the information of the gas opacity of all molecules that are photoprocessed by cosmic ray induced UV photons in our chemical evolution model. By studying the impact that the gas opacity of individual species has on the chemistry and viceversa, we can build a simplified tool that includes the most important species while understanding the underlying relationship between the opacity and the chemistry. As some opacities rise, an important shielding effect appears and the CRUV photoprocess rates change. This affects the chemical formation pathways for both gas and ice phase species.

The most important species that contribute to the gas opacity are O₂, SiO, Si, CO and CO₂, in a consistent manner throughout the 1–8 AU region of the disk midplane. We find that the opacities of O₂, SiO (and CO₂ in the warm regions around 1 AU) are the most variable in time and hence are the ones that require most attention, and whose effects cannot be easily dismissed. As the CO and S abundances remain more or less constant in those regions, their opacity remains fairly constant as well. Thus, future models must include this treatment of CRUV gas and dust opacity while only considering the contribution of the most significant species that our models yield for the probed regions of the disk.

Finally, we found that if SiO is steadily created in the midplane at long timescales, it can drift vertically upwards and accumulate around the $A_V = 1$ region, thus suggesting a possibility for future detections of SiO in protoplanetary disks.

References

1. Aikawa, Y. 2007, *ApJL*, 656, L93
2. Aikawa, Y., Miyama, S. M., Nakano, T., & Umebayashi, T. 1996, *ApJ*, 467, 684
3. Bockelée-Morvan, D., Crovisier, J., Mumma, M. J., & Weaver, H. A. 2004, *The composition of cometary volatiles*, ed. Festou, M. C., Keller, H. U., & Weaver, H. A., 391–423
4. Bockelée-Morvan, G. 2010, in *Physics and Astrophysics of Planetary Systems*, EAS Publication Series No. 41, 313–324
5. Brown, P. N., Byrne, G. D., & Hindmarsh, A. C. 1989, *SIAM J. Sci. Stat. Comput.*, 10, 1038

6. Cazaux, S. & Tielens, A. G. G. M. 2002, *ApJL*, 575, L29
7. Chaparro Molano, G. & Kamp, I. 2012, *A&A*, 537, A138
8. D'Alessio, P., Calvet, N., & Hartmann, L. 2001, *ApJ*, 553, 321
9. Fedele, D., van den Ancker, M. E., Henning, T., Jayawardhana, R., & Oliveira, J. M. 2010, *A&A*, 510, A72
10. Gredel, R., Lepp, S., Dalgarno, A., & Herbst, E. 1989, *ApJ*, 347, 289
11. Hasegawa, T. I. & Herbst, E. 1993, *MNRAS*, 261, 83
12. Jenkins, E. B. 2009, *ApJ*, 700, 1299
13. Leger, A., Jura, M., & Omont, A. 1985, *A&A*, 144, 147
14. Öberg, K. I., van Dishoeck, E. F., & Linnartz, H. 2009, *A&A*, 496, 281
15. Prasad, S. S. & Tarafdar, S. P. 1983, *ApJ*, 267, 603
16. R. Riahi, Ph. Teulet, Z. Ben Lakhdar, & A. Gleizes. 2006, *Eur. Phys. J. D*, 40, 223
17. Roberts, J. F., Rawlings, J. M. C., Viti, S., & Williams, D. A. 2007, *MNRAS*, 382, 733
18. Semenov, D., Hersant, F., Wakelam, V., et al. 2010, *A&A*, 522, A42
19. Semenov, D., Wiebe, D., & Henning, T. 2004, *A&A*, 417, 93
20. Shen, C. J., Greenberg, J. M., Schutte, W. A., & van Dishoeck, E. F. 2004, *A&A*, 415, 203
21. Sternberg, A., Dalgarno, A., & Lepp, S. 1987, *ApJ*, 320, 676
22. Thi, W.-F., Woitke, P., & Kamp, I. 2011, *MNRAS*, 412, 711
23. Umebayashi, T. & Nakano, T. 1981, *PASJ*, 33, 617
24. Visser, R., Doty, S. D., & van Dishoeck, E. F. 2011, *A&A*, 534, A132
25. Visser, R., van Dishoeck, E. F., Doty, S. D., & Dullemond, C. P. 2009, *A&A*, 495, 881
26. Walsh, C., Millar, T. J., & Nomura, H. 2010, *ApJ*, 722, 1607
27. Woitke, P., Kamp, I., & Thi, W. 2009, *A&A*, 501, 383
28. Woodall, J., Agúndez, M., Markwick-Kemper, A. J., & Millar, T. J. 2007, *A&A*, 466, 1197